Electronic Journal of Structural Engineering

Original Article

Cite this: DOI:10.56748/ejse.24532

Received Date: 09 October 2023
Accepted Date: 03 January 2024

1443-9255
https://ejsei.com/ejse

Study on the dynamic construction mechanics of side piles in metro station using the pile-beam-arch method

Xingzhong Nong[a], Xingkai Pei[a], Shuai Zhang[b], Gongning Liu[b*]

[a] Guangzhou Metro Design & Research Institute Co., Ltd, Guangzhou, Guangdong 510010, China.

[b] Southwest Jiaotong University, Key Laboratory of Transportation Tunnel Engineering, Ministry of Education, Chengdu, No. 111, North Section, Second Ring Road, Jinniu District, 610031, China.

*Corresponding author: 2995484603@qq.com

Abstract

Based on the Tianhe East Station in Guangzhou Metro Line 11 engineering, this paper analyzes the formation mechanism of soil arching effect (SAE) of station by pile-beam-arch (PBA) method in the excavation process and studies the mechanics and deformation laws of side piles in different construction stages under different pile spacing conditions. The results show that the formation, development, and destruction of SAE between side piles are closely related to the construction process. Both too large and too small pile spacings are not conducive to the development of SAE between piles; when it is located between them, the SAE between piles exerts greatly. In the form of a composite lining system, side piles as well as SAE between side piles play an effective role in supporting the soil behind piles. The lateral deformation of pile body is the most significant in the completion of buckle arch to the excavation of the first soil layer, which is the critical construction phase to reduce lateral deformation of side pile. The axial force of side pile increases gradually with the excavation of station, and the change is the most drastic at the excavation stage of the first soil layer. The influence of pile spacings on vertical settlement and axial force of side piles is much greater than that of the horizontal displacement and bending moment.

Keywords

PBA method, Side pile, Construction mechanics, Deformation law, Internal force

1. Introduction

Metro provides great convenience for people to travel on daily life, and the deformation and mechanical characteristics of metro in the construction process have attracted much attention (Huang et al. 2022; Sun et al. 2023; Wang et al. 2023). The PBA method is conductive to control the surface deformation as well as reduce the influence of construction on the surrounding buildings, the PBA method develops rapidly. It has been greatly adopted in the construction of many domestic metro stations, and gradually became a vital construction method for urban subway construction. The existing studies mainly focused on the stratum deformation caused by metro construction with the PBA method and proposed corresponding control measures (Guo et al. 2021; Zhao et al. 2022; Liu and Huang 2023; Li et al. 2023), indicating that the stratum deformation led by the excavation of guide tunnel and the top buckle arch occupied the main part. Therefore, these two construction stages should be paid more attention to control the stratum settlement, and better control effect can be achieved by shortening the excavation footage, setting transverse linings, injecting grouting behind the preliminary lining, and advanced small pipe grouting reinforcement in the arch (Liu et al. 2013; Hu 2016; Yu et al. 2019; Lv et al. 2023). On the other hand, the scholars also studied the force and deformation of station structure with PBA method. Luo (2021) pointed out that in the metro construction using PBA method, the mechanical transformation of beam-arch-column structure occurred for many times, and the stress variation amplitude of all stressed members reached the maximum in the buckle arch construction stage, and the peak stress of other members except the maximum compressive stress of side pile occurred in the buckle arch construction stage. Liu et al (2017) simulated all construction phases about metro using PBA method through the comparison and analysis of two kinds of secondary lining construction methods and found that that the construction of secondary lining using the top-down method can reduce the surface deformation as well as the internal force in the lining structures obviously during the excavation inside the station. Zhang (2018) pointed out that in the excavation process of PBA method, the arch structure, retaining pile and central steel pipe column constituted the overall force system, and the retaining pile eventually played a dominant part in the force of frame systems.

On the other hand, in the design of supporting pile structure, the interaction of pile-soil is usually separated, and the soil is only regarded as the load, while the supporting pile is regarded as a mechanical structure, without considering the interaction between the two. There is a mutual influence relationship between piles and soil, so the supporting piles and soil should be regarded as a common supporting system. Soil is both the load and the carrier, and the self-bearing capacity of soil is mainly manifested as SAE. At present, research on the SAE between piles or deformation of piles mainly focus on piled embankments (Zhuang et al. 2018; Lai et al. 2018; Rui et al. 2022), composite foundations, slopes, and foundation pits (Kahyaoğlu et al. 2012; Chen et al. 2016; Cheng et al. 2020; Liu and Yu 2022), while there is few research on the SAE caused by side piles of station by PBA method with complex stress state. Zhu et al. (2014) analyzed the mechanism of the SAE of cushions in pile foundations, and found that the greater the cushion thickness, the more significant the SAE formed by a cushion. The friction coefficient and porosity of soil had a great influence on the SAE, but pile diameter showed a slight influence on SAE. Relying on the deep foundation pit project in the loess layer, Wang (2017) discussed the generation, development as well as destruction process of the SAE under the deep foundation pit with supporting piles, and further studied the impact of pile spacings, foundation pit depths, and soil properties on the SAE. Lai et al. (2014) carried out a simulation study on SAE of embankments, verified the existence of SAE, and analyzed the formation and development process of the SAE as well as the mechanical transfer mechanism generated by it based on mechanics. Zhao et al. (2016) analyzed the impact of horizontal SAE between piles on the force of the composite structure between piles and walls, deduced the force calculation method of piles and retaining walls in the composite structure when the SAE is considered, and verified the rationality of the method based on the actual slope case. Li et al. (2018) found that when SAE was considered, the longitudinal force of anti-slide piles increased significantly while that of soil nailing wall decreased significantly, which greatly saved the amount of soil nailing. Zhang et al. (2023) studied the rule of SAE of pile-supported foundation pit and found that with the increase in pile spacings, SAE is less significant. The enlargement of friction coefficients was not conducive to the change of soil arch shape, while it can significantly increase the efficiency of load transfer.

At the same time, underground engineering construction is closely related to the geological conditions. The strata in Guangzhou area are complicated, and the project construction related to subway station with the PBA method has not been carried out yet, so there is a lack of mature construction experience. Relying on the Tianhe East Station of Guangzhou Metro Line 11 by PBA method, this paper studies the formation and change laws of SAE between piles caused by side piles and analyzes the mechanics and deformation law of side piles in different construction stages, which may provide certain basis for the design and construction of similar side piles of station by PBA method.

2. Engineering background

Guangzhou Metro Line 11 is a downtown metro loop with a total length of 43.2km, as displayed in Fig. 1. Among them, Tianhe East Station, Shahe Station, Liuhua Road Station and Huajing Road Station in the project of Line 11 are all constructed by PBA method. The Tianhe East Station project, which is mainly located in the weakest geological conditions (strongly weathered strata), is studied in this paper. Tianhe East Station is a one-column and two-span structure, and the underground two floors are all underground stations, which are constructed by the PBA method. The adopted side piles are manual excavation piles with a diameter of 1.2m, pile spacing of 1.5m and length of 15m according to on-site material. The lateral section of the station structure is displayed in Fig. 2.

Fig. 1 Location of the Guangzhou Metro Line 11 Project

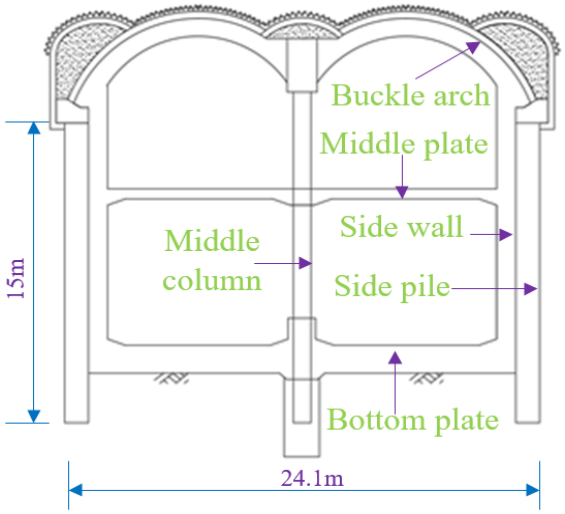

Fig. 2 Cross section of the station structure

3. Numerical calculation instructions

3.1 Calculation model

FLAC3D is adopted for the calculation and analysis. The relevant physical and geometric parameters of the calculation model are calculated according to the actual engineering data of Guangzhou Metro Line 11. The calculation model is displayed in Fig. 3. To ensure the precision of numerical calculation as well as reduce the effect of the "boundary effect" on the calculation results, the model size is set as $width \times height \times longitudinal$ length=$72m \times 35m \times 21m$. The normal displacement constraint is applied to the bottom and surrounding boundaries of the model, and the load is imposed on the top surface to simulate the actual engineering depth. The upper part of the soil layer is highly weathered argillaceous siltstone, and the lower part of the soil layer is breezy gravel coarse sandstone.

To investigate the impact of target factors on side piles of station with the PBA method more specifically, the model is simplified based on the mechanical equivalence principle, and the buckle arch force (F_{arch}) of station arch is equivalent to decomposed into vertical load (F_x) and horizontal load (F_y) imposed on the crown beam and middle column. Meanwhile, uniform soil load (q) is applied to the soil surface behind the piles to simulate the overlying soil load. The simplified model diagram is displayed in Fig. 4. According to the calculation result of the bedded-beam model, the obtained F_y and F_x on the crown beam structure bear are 1200kN/m and 800kN/m, respectively. The middle column bears the vertical load of the left and right buckle arches within the spacing range of 8m columns. The horizontal loads counteract each other due to the symmetry of the left-right arches. The obtained q behind the pile is 250kPa.

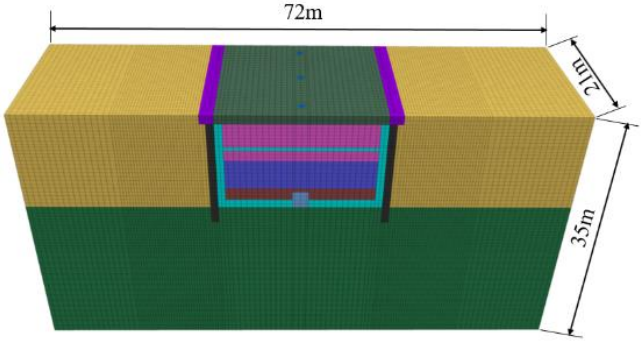

Fig. 3 Calculation model

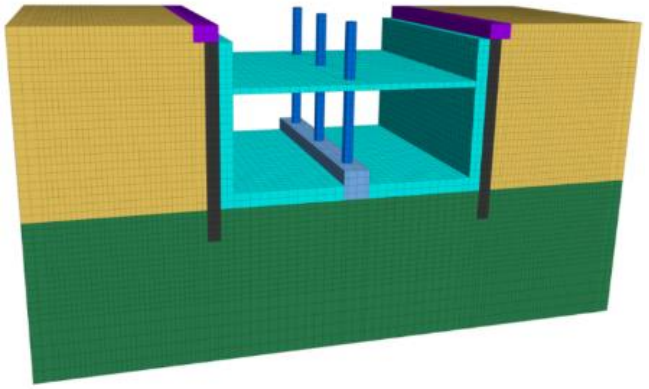

(a) Station model

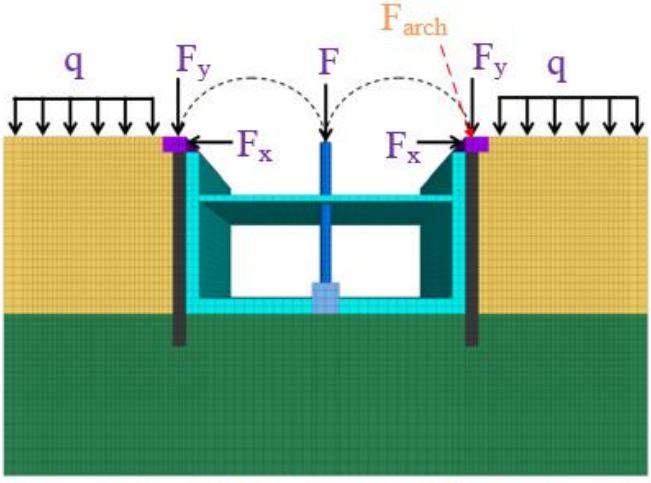

(b) Load simplification

Fig. 4 Model simplification diagram

3.2 Calculation parameters

The soil as well as lining structure is calculated using solid elements, and the surrounding rock is simulated by an ideal elastic-plastic constitutive model, which obeys the Mohr-Coulomb strength yield criterion. The lining structure is regarded as a linear elastic material, and an elastic constitutive model is used. The calculation parameters of surrounding rock as well as lining structure are displayed in Table 1.

For the simulation of side piles in the metro using the PBA method, the built-in pile structure elements in FLAC3D are used to realize the interaction between piles and soil. The coupling springs at each node of pile elements are adopted to realize the interaction between the grids of the surrounding soil, and the force and deformation are transmitted through the normal and tangential coupling springs. In this way, the tangential friction between piles and soil can be reflected as well as the normal compression effect of soil around piles on pile body, which more appropriately realizes the coupling effect of pile-soil (Luo et al. 2007; Chen and Xu 2013). The mechanical relationship of tangential coupled springs at pile-soil contact surface is shown in Fig. 5.

Table 1 Calculation parameters

Name	Component	Material	Size	Density (kg/m³)	Elastic modulus - E (GPa)	Poisson's ratio - μ	Cohesion (kPa)	Friction angle (°)
Highly weathered argillaceous siltstone	-	-	-	2100	0.12	0.33	50	28
Breezy gravel coarse sandstone	-	-	-	2600	2	0.25	260	32
Lining structure	Crown beam	C30 RC	1.8×1.2m	2500	30.0	0.20	-	-
	Center column	Q355B +C50 RC	0.9m@8m	2700	63.5	0.20	-	-
	Bottom beam	C35 RC	1.4×2.9m	2700	31.5	0.20	-	-
	Sidewall	C35 RC	0.8m	2700	31.5	0.20	-	-
	Muddle plate	C35 RC	0.5m	2700	31.5	0.20	-	-
	Bottom plate	C35 RC	1.2m	2700	31.5	0.20	-	-

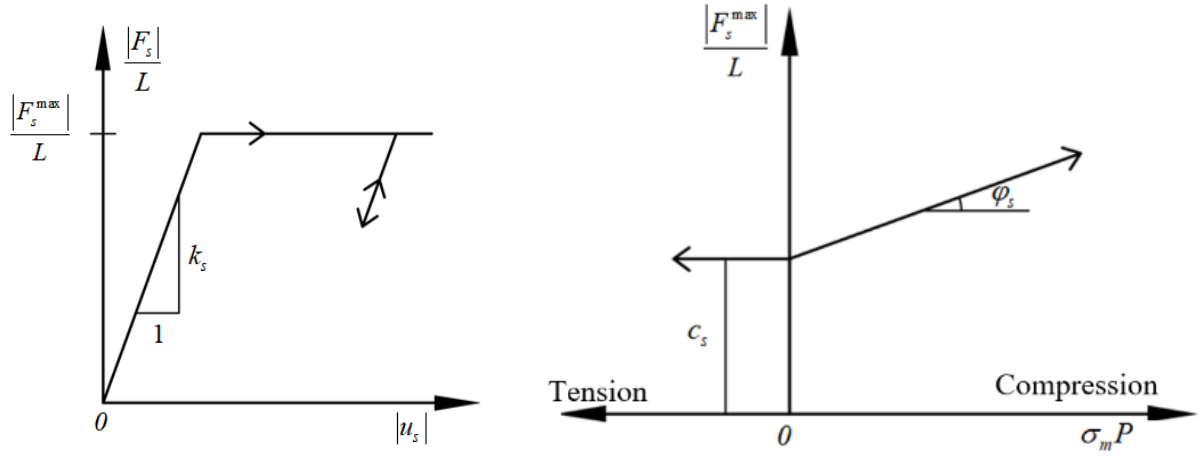

(a) Shear force and relative shear displacement (b) Shear strength criterion

Fig. 5 Mechanical relationship of tangential coupling spring on pile-soil interface

Table 2 Parameters of Pile-Soil Coupling Springs

Name	Elastic modulus (GPa)	Tangential coupled spring			Normal coupled spring		
		Stiffness (Pa·m⁻¹)	Cohesion (Pa)	Friction angle (°)	Stiffness (Pa·m⁻¹)	Cohesion (Pa)	Friction angle (°)
Side pile	30.0	1.0×10^{11}	4.0×10^{4}	22.4	1.0×10^{11}	4.0×10^{4}	22.4

The shear strength of pile-soil contact surfaces is primarily influenced by natural bonding properties as well as friction force. The shear force formed through pile-soil relative displacements is represented through the stiffness of shear coupling springs, expressed by Eq. (1).

$$\frac{F_s}{L} = k_s(u_p - u_m) \quad (1)$$

Where: F_s refers to the shear force formed by the shear coupling springs; L refers to the element action length; k_s refers to the stiffness of shear coupling springs per unit length; u_p refers to the axial displacement about pile body; u_m refers to the axial displacement about the soil mass.

The maximum possible shear force along the contact surface of piles and grids is relevant to the bonding strength as well as friction force of the interface, and the maximum shear force per unit length of piles is expressed as Eq. (2).

$$\frac{F_s^{max}}{L} = C_s + \tan(\varphi_s)\,\sigma_m P \quad (2)$$

Where C_s is the bonding force of the shear-coupled springs; φ_s is the friction angle of the shear-coupled springs; σ_m is the normal effective lateral limiting stress of piles; P is the outer ring circumference of the piles.

Because the mechanics of normal coupled spring stiffness are like the strength criterion of tangential coupled spring stiffness above, it will not be restated here. Concerning relevant literature (Liu and Han 2010; Chen and Xu 2013) and multiple trial calculations by FLAC3D, the coupled spring parameters of pile elements are displayed in Table 2.

3.3 Simulation of the construction process

The construction process of numerical analysis is simulated according to the actual construction process of Guangzhou Metro station with the PBA method. The specific simulation steps are as follows:

(1) Generate the initial ground stress field.
(2) Install the side piles, crown beam and middle column structure.
(3) Apply the buckling force of the arch structure (i.e., F_x and F_y) to the crown beam and F to the middle column structure.
(4) Excavate the first soil layer of the main body of the station.
(5) Install the middle plate and the upper side wall structure of the station.
(6) Excavate the second soil layer of the main body of the station.
(7) Excavate the third soil layer of the main body of the station.
(8) Install the bottom plate, bottom longitudinal beam and lower side wall structure, and the construction of the main structure of the station is completed.

4. Analysis of the calculation result

4.1 SAE between side piles

4.1.1 The influence of Pile Spacing

To directly obtain the force transmission path and distribution rule of the SAE between side piles, the X-direction stress vector diagram of soil mass during the formation of SAE is extracted, as displayed in Fig. 6.

As can be seen from the stress vector diagram of soil between side piles in Fig. 6, the soil stress is deflected in the direction of transmission in the yellow "soil arch" stress zone and transferred to the side piles along the soil arch trace line, that is, the soil arch zone has an effective shield and protection effect on the soil between side piles, making the side piles bear most of the soil pressure. The soil in the stress dissipation area in red hardly bears the stress of the external soil, which indicates that the SAE is relatively significant currently.

To compare the difference in SAE under various pile spacings, the X-direction stress cloud map of soil behind the side piles when the SAE is formed under the pile spacings of 1.25D, 2.5D, 5D and 7.5D is extracted respectively (D refers to the pile diameter), as shown in Fig. 7.

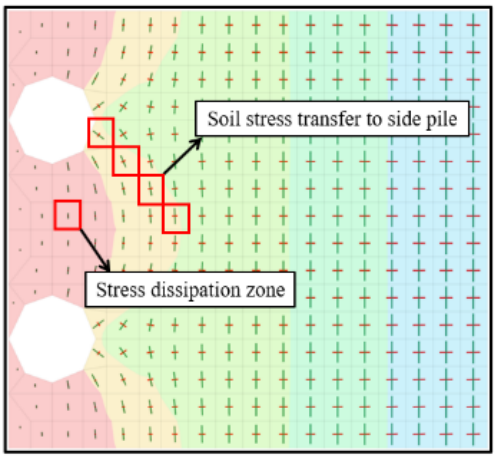

Fig. 6 Distribution law of the X-direction stress vector of the soil between side piles

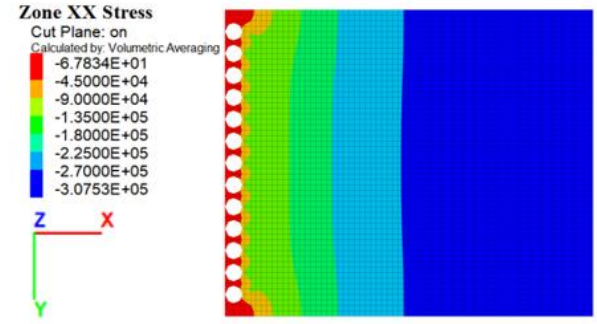

(a) Pile spacing =1.25D

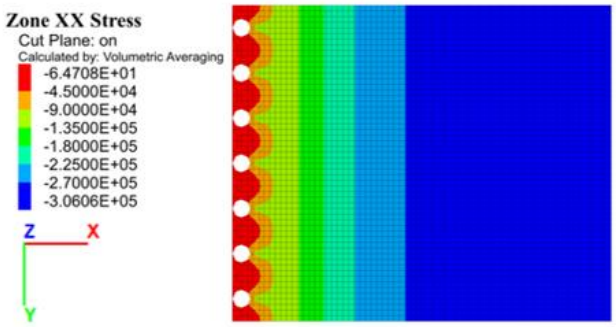

(b) Pile spacing =2.5D

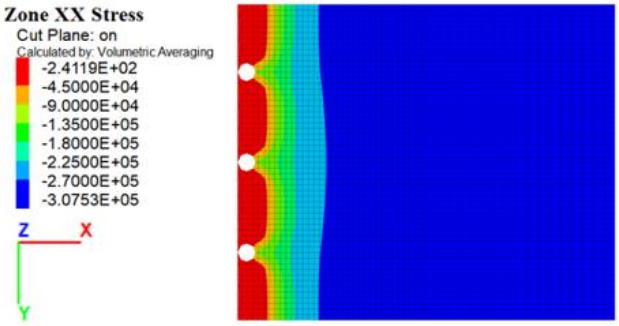

(c) Pile spacing =5D

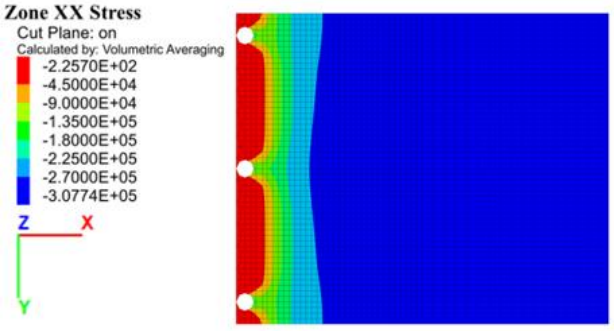

(d) Pile spacing =7.5D

Fig. 7 X-direction stress cloud map of post-pile soil under different side pile spacings

In Fig. 7, when the pile spacings are 1.25D, 2.5D, 5D and 7.5D, there are arch stress zones and stress dissipation zones between the two side piles, indicating that an effective soil arching is generated between the side piles, namely, the SAE between the side piles. However, when pile spacing is 1.25D, due to the little pile spacing, the side pile mainly relies on the pile itself to directly block the soil behind the piles, and the lateral isolation supporting ability is excessive. The SAE is not fully utilized and only exists in a minimal range behind the piles, and the stress dissipation area between piles is small. When increasing the pile spacing, an obvious stress concentration zone is formed in a certain area behind the piles, and the extension range of the stress dissipation zone between the piles increases. The SAE between the piles plays an effective supporting role on the soil behind the piles in the form of a composite support system. However, when the pile spacing is large, that is, the pile spacing is 7.5D, the range of soil deformation constrained by the soil arching structure between piles continues to increase, the soil arching structure is gradually flattened, the soil arch shape changes from the original "pointed arch" to "flat arch", and the arch foot position of soil arching structure changes from the back of the pile body to the side of the pile body. The soil stress behind the piles will flow around the pile body. The stresses in soil are difficult to be transferred to the side piles through the arch structure between piles and the arch effect of native soil gradually disappears. At this time, the side piles cannot form the pile-soil composite retaining effect, and only relies on the side piles itself to directly support the soil behind piles, that is, to reduce the longitudinal span of soil excavation-free surface at the station, which is easy to occur the instability of the supporting surface and other hazards.

In conclusion, if pile spacing is little (only 1.25D), the isolation ability of side piles is too strong, and the SAE between side piles exists but is difficult to exert fully. In this case, the lateral support effect between piles is mainly based on the side piles, while the SAE between side piles is auxiliary. When the distance between piles is large (more than 7.5D), the soil arch between side piles exceeds the bearing limit and is destroyed, the SAE disappears, and the soil stress behind side piles flows around the pile body. In this case, the pile-soil lateral retaining effect only depends on the direct retaining effect of the side piles itself, which plays a role of "longitudinal span reduction" on the free surface of soil excavation. If pile spacings are between the two, the pile-soil lateral retaining action is in the middle equilibrium state, and the SAE and longitudinal span reduction between the side piles have both effects, and the retaining ability is fully brought into play, the composite supporting system is used to effectively support the soil behind the side piles.

Therefore, in practical engineering applications, to fully exert the SAE, the spacing of side piles should be reasonable. Too large pile spacing is easy to cause structural instability, and too small pile spacing will cause poor engineering economy. Taking into account the strength of SAE as well as the requirement of pile spacing, pile spacing 2.5D is recommended in this paper.

4.1.2 Evolution laws of SAE between piles with construction process

To reveal the formation as well as evolution laws of SAE between side piles at different construction stages of a subway station with PBA method, the condition with the most significant SAE between piles is extracted (i.e., the pile spacing 2.5D), and the X-direction stress distribution characteristics of soil behind side piles at different excavation depths and construction stages are analyzed, as shown in Table 3. The main research sections are Section 1 (-2.50m depth from the pile top) and Section 2 (-7.50m depth from the pile top). To compare the development laws of soil stress in different construction stages, the legend of stress nephogram is processed uniformly in this paper.

In Table 3, for Section 1, after the completion of buckle arch construction of the side piles, there exists a certain stress concentration phenomenon in the soil behind the piles. This is because the piles produce active positive displacement under the action of the buckle arch at the top, thus squeezing the soil behind piles, and the soil behind the piles resizes the deformation by generating passive soil pressure. As a result, the X-stress of soil behind piles is greater than that between piles, forming an active arch stress circle. For Section 2, the stress distribution is almost linear and does not change obviously because the relative displacement difference between the soil behind and between piles is small. Therefore, the generation of soil relative displacement is crucial to the formation of SAE.

During the excavation in the first soil layer of station, the soil behind the piles has a certain deformation, and the side piles are squeezed, and the active soil pressure is generated. An obvious "arch" stress zone appears near the side pile structure at a depth of -2.50m near excavation faces. In addition, there is a red stress dissipation zone in the soil between side piles, and the stresses in the soil of X-direction reduce rapidly within this range. There is a yellow "arch" stress concentration zone behind the piles, and the soil stress deflecting. The soil in this part is transferring the

Table 3 Stress nephogram of the soil behind side piles in X direction /Pa

Construction stage	Section 1	Section 2
Completion of the buckle arch	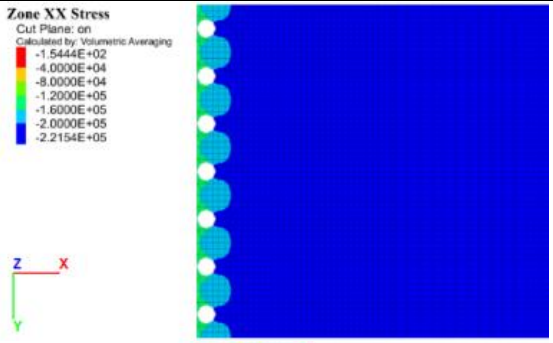	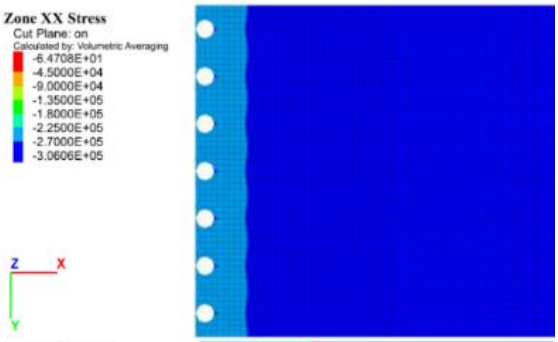
Excavation of the first layer	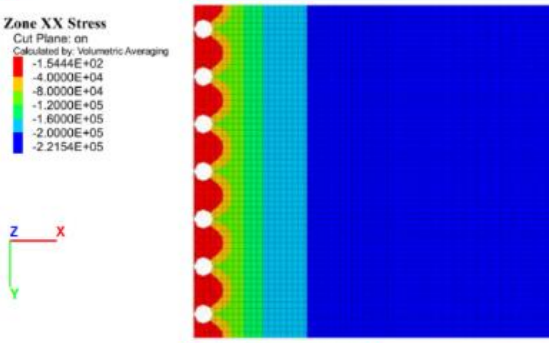	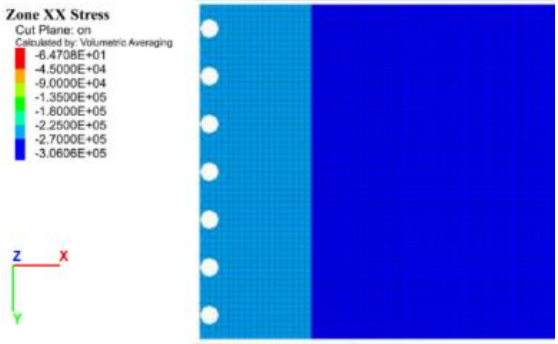
Excavation of the second layer	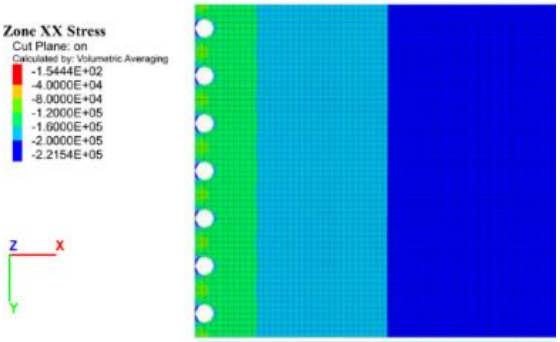	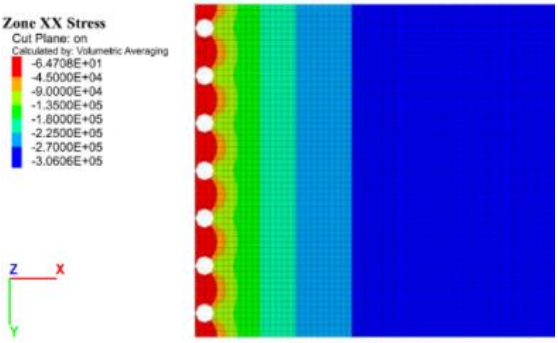
Completion of the bottom plate	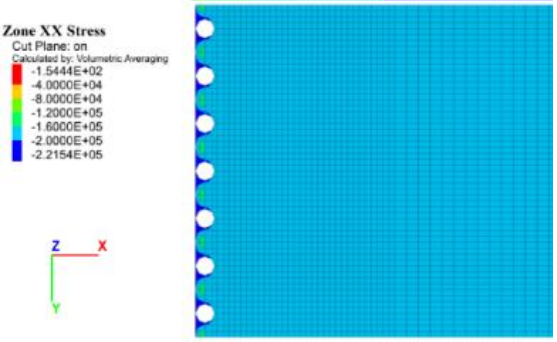	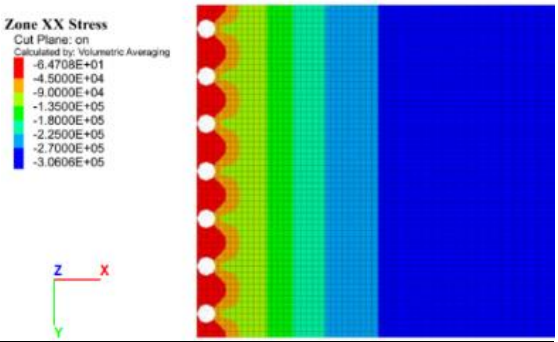

soil stress behind the arch to the side piles through the arch foot, indicating that an effective "arch effect" is formed here.

With the progress of station construction, the excavation surface of soil keeps moving down, and the SAE of soil behind piles also moves downward. The SAE of shallow soil gradually disappears, and the SAE between piles gradually appears in Section 2 after soil excavation, which also shows that the formation, development, and destruction of SAE between side piles are closely related to the construction process. The horizontal SAE between side piles is mainly formed in the area where the relative displacement of soil near the excavation face is large.

4.2 Mechanical properties and deformation law of side piles during construction

4.2.1 Analysis of the deformation of side piles

The evolution laws of lateral displacements of side piles under different pile spacings with the construction process are extracted, as displayed in Fig. 8. Meanwhile, the maximum lateral displacements of side piles under various construction phases are listed, as displayed in Table 4. For the convenience of description, the lateral displacement of side piles to the outer direction of the station is regarded as the forward direction.

In Fig. 8, the overall variation trend of the lateral displacement of side piles under different pile spacings is basically the same. After the top buckle arch is completed, the side piles resemble the cantilever beam. The pile body first generates a "forward type" positive displacement away from the station structure. The largest lateral displacement of the pile body is located at the pile top, and the displacement value can reach 5.91 ~ 7.05mm, and the positive displacement increases with the pile spacings. The main reason is that the arch structure transfers the upper pressure to side piles through the crown beam, which generates horizontal thrust to the side piles outside the station, making the top of side piles offset to the outside of the station. Meanwhile, with the increase of pile spacings, the pile foundation embedment is weakened, and the displacement gradually increases.

Subsequently, due to the unloading effect led by the constant downward excavation of soil in the metro, the soil stress differences between the inside and outside side piles gradually increase, and the side piles gradually shift to the inside of the station. However, due to the horizontal constraint effect of the buckle arch force on the pile top, the lateral deformation of pile body changes into a "bulging" deformation characteristic with great value at the middle and small value at both ends, which rapidly decreases in the embedded stratum at the bottom of the station approaching to 0mm. In addition, the lateral displacement of side piles increases gradually with the downward movement of the free surface of soil excavation, and the location of the largest lateral displacement of side piles moves downward.

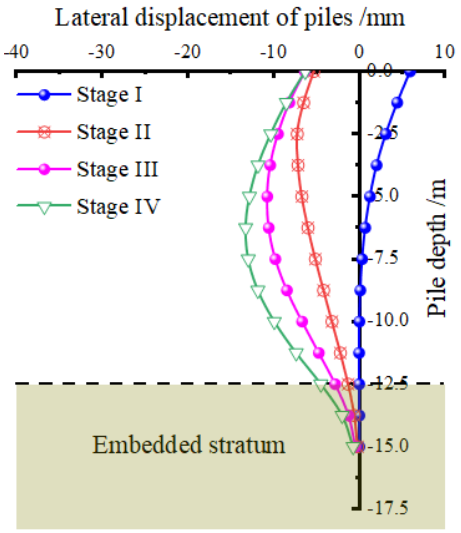

(a) Pile spacing =1.25D

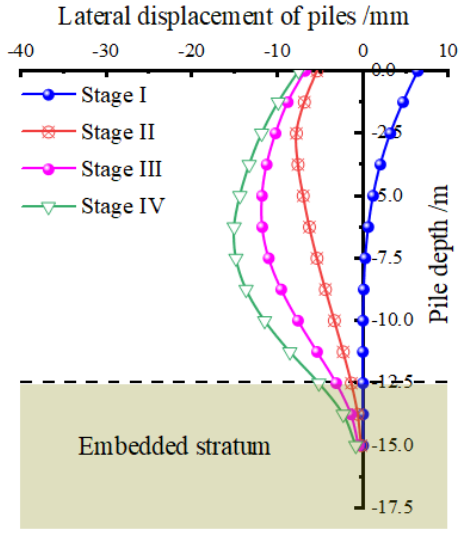

(b) Pile spacing =2.5D

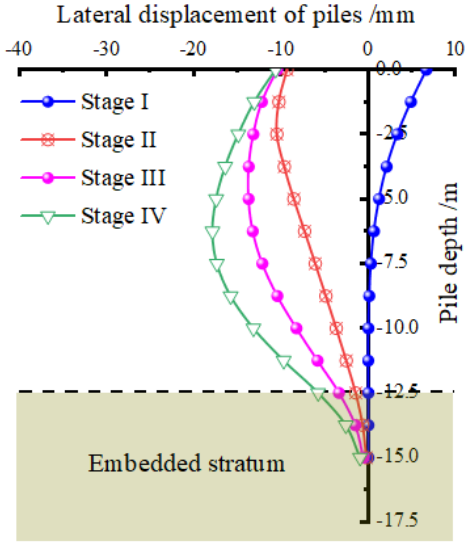

(c) Pile spacing =5D

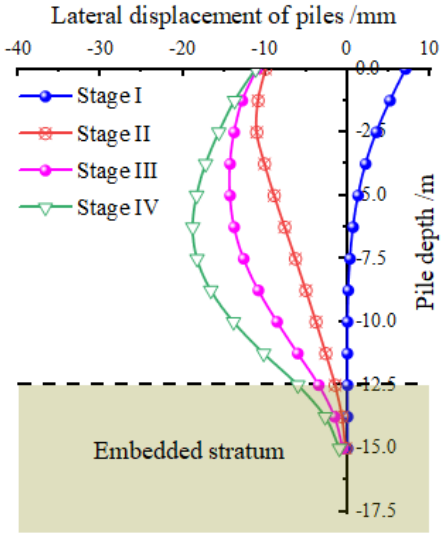

(d) Pile spacing =7.5D

Fig. 8 Evolution law of lateral displacement of side piles with the construction stages

Note: Stage I refers to the completion of buckle arch; Stage II refers to the excavation of the first layer; Stage III refers to the excavation of the second layer; Stage IV refers to the completion of the bottom plate.

Table 4 Maximum lateral displacement of side piles during station construction /mm

Pile spacing	Construction stage			
	Completion of the buckle arch	Excavation of the first soil layer	Excavation of the second soil layer	Completion of the bottom plate
1.25D	5.91	-7.26	-10.75	-13.27
2.5D	6.39	-7.42	-11.82	-15.06
5D	6.65	-10.48	-13.72	-17.86
7.5D	7.05	-11.05	-14.29	-18.82

In Table 4, the lateral displacement of the pile body changes most dramatically from the completion of buckling arch to the excavation of the first soil layer. Currently, because of the excavation as well as the unloading about soil inside the station, the side piles are subjected to the lateral stress about soil behind the side piles, and side piles bear large lateral displacement. The positive displacement toward the outside of the station quickly changes to the negative displacement toward the inside station. The largest change values in this stage can reach 18.1mm, with a large range of change, indicating that this process is the crucial phase to reduce the lateral deformation of side piles, which is basically consistent with the conclusion of previous literature (Han et al. 2015). Due to the timely application of the middle plate in the station, the lateral displacements of pile body led by the subsequent soil excavations in the station are obviously controlled, and the displacement change rate begins to slow down, indicating that the slab structure is vital to controlling the lateral deformation of side piles as well as the stability of the structure. It is suggested to apply the middle plate in time during the station construction.

To reveal the impact rule of pile spacings more directly on the lateral displacement of side piles, the final lateral displacement comparison diagrams of side piles under different pile spacings after station construction are drawn, as displayed in Fig. 9.

In Fig. 9, the lateral displacement of the side pile increases with pile spacings, and the final lateral deformation of pile body presents a "bulging" deformation feature with large values at the middle as well as small values at both ends, and the largest lateral displacements locate at the middle of pile body. However, when pile spacing exceeds 5D, the increased rate about lateral displacements of side piles slows down significantly. Compared with the largest lateral displacement of side piles (17.86mm for pile spacing 5D) and (18.82mm for pile spacing 7.5D) and the displacement increment reaches 0.96mm, it indicates that when pile spacing exceeds a certain range, the lateral deformation of side piles no longer increases significantly.

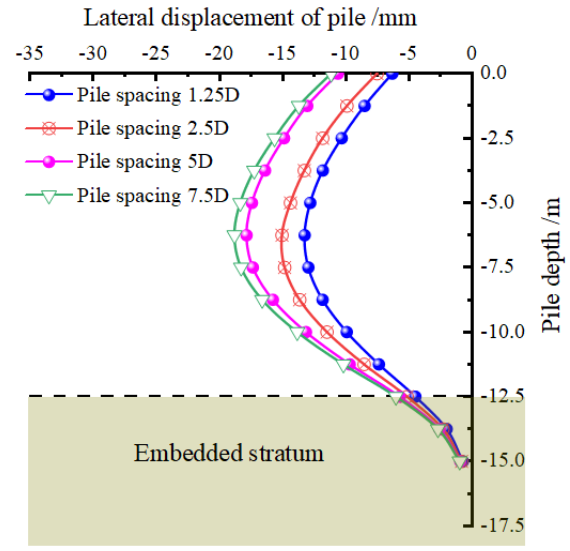

(a) Distribution diagram of the lateral displacement of side piles

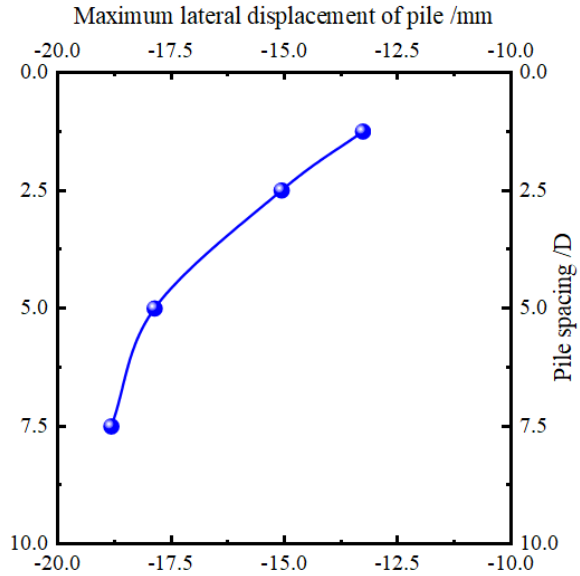

(b) Variation curve of the maximum lateral displacement of side piles with pile spacings

Fig. 9 Final lateral displacement comparison diagram of side piles with different pile spacings

The construction process of the station using the PBA method involves much structural mechanical transformation, among which the most critical part is that the forces of the arch structure are transferred to the side piles, so the displacements of pile top connecting the side piles and arch structure are particularly important. When the pile top deformation is too large, it is easy to cause the failure and detachment of the connecting nodes, resulting in the failure and instability of the station. The final vertical settlement and horizontal displacement of pile top after the station construction under different pile spacings are displayed in Fig. 10.

In Fig. 10, with the increase of pile spacings, the vertical settlement about pile top presents a trend of rapid increase. This is because the soil strength of highly weathered strata is weak, and the vertical load of arch structure is almost all borne by side piles. As the pile spacings increase, the number of side piles below the unit distance decreases, so the vertical load carried by a single pile increases, and the vertical settlements about the pile top also increase. The horizontal displacement about pile top increases with the pile spacings, but the increased rate decreases gradually. This is because the horizontal thrust of the buttoning arch of the pile top constrains the lateral deformation about the pile top to some extent, which restrains the continuous increase of the lateral deformation about pile top. When pile spacing is 1.25D, the vertical and horizontal displacements about the pile top are -8.09mm and -6.33mm, respectively. When the pile spacing increases to 7.5D, the vertical and horizontal deformation about pile top increase by 47.30mm and 4.84mm, respectively, compared with the pile spacing is 1.25D. The increased rates of vertical settlement and horizontal displacement are 584.67% and 76.46%, respectively, showing that the impact about pile spacings on vertical settlement of side piles is much larger than that of the horizontal displacement.

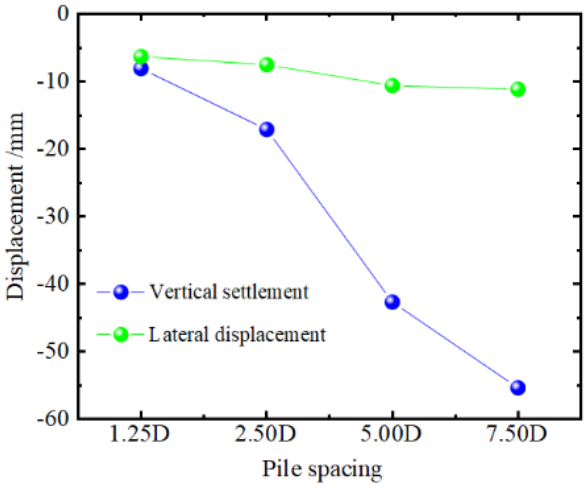

Fig. 10 Curve about the final deformation of the pile top with different pile spacings

4.2.2 Analysis of the change law of the internal force of side piles

The evolution diagram of the internal force of side piles under different pile spacings during the construction process is extracted respectively in Table 5, and the comparison diagram of internal force of side piles under different pile spacings after the station construction is drawn, as displayed in Fig. 11.

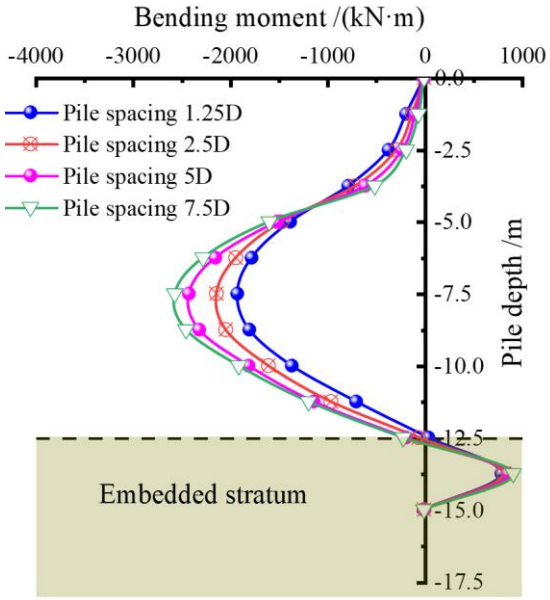

(a) Bending moment

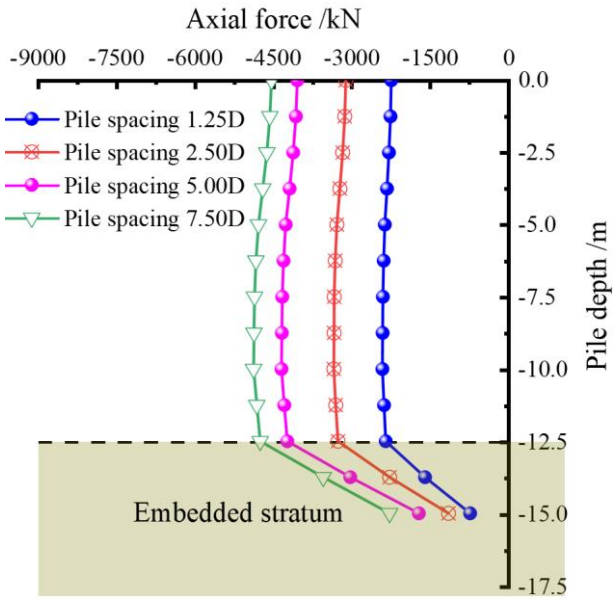

(b) Axial force

Fig. 11 Comparison of the final internal force of side piles with different pile spacings

Table 5 Evolution diagram of internal forces about pile body

Pile spacing	Distribution characteristics of the bending moment	Distribution characteristics of the axial force
1.25D	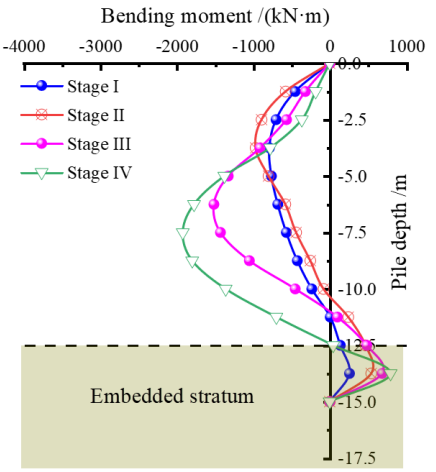	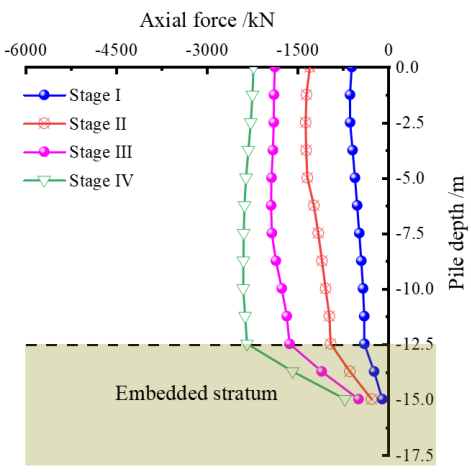
2.5D	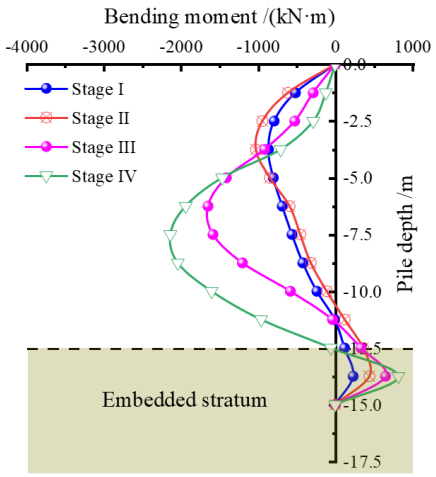	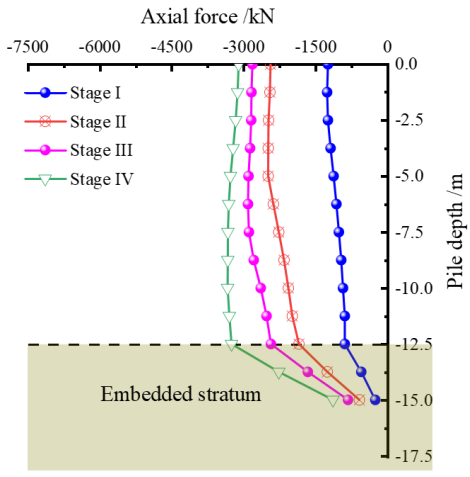
5D	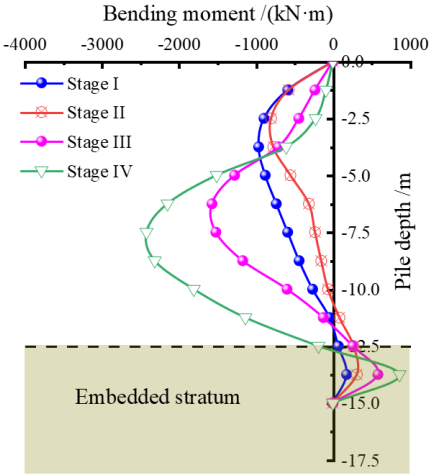	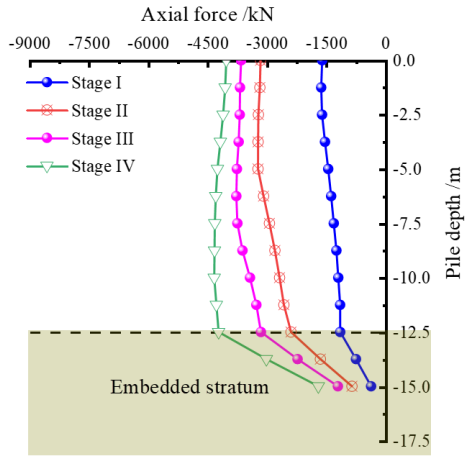
7.5D	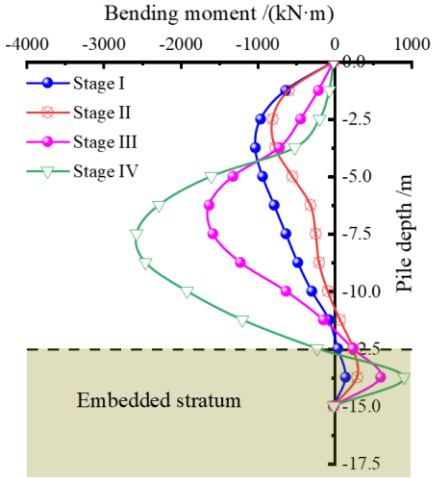	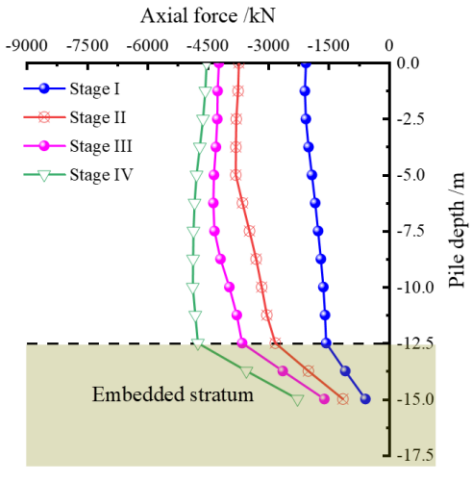

In Table 5, for the distribution of the bending moment of side piles, it presents a "bow" distribution with a large value at the middle and a small value at both ends. The side piles above the soil excavation surface are mainly strained on the excavation side of the station, while the side piles embedded in the lower rock layer is mainly strained on the side facing the soil behind the piles. The position about the section of the largest bending moment moves down with the continuous downward excavation about soil, which matches the lateral deformation law of the side piles. In addition, the bending moment about the upper part of side piles decreases after the excavation of the first soil layer. This is due to the timely application about middle plate and upper sidewall structure, which is equivalent to the addition of supporting and resisting external force inside the side piles, shows a better-supporting effect on upper section about side piles, inhibits the lateral deformation of the upper part about piles, and reduces the bending moment about upper part of the side piles, and effectively controls the internal force of side piles. In terms of the axial forces distribution about side piles, the axial forces of side piles present a "fold line" form with large at the top and small at the bottom. The axial force changes at the interface between soil excavation surface and stratum. In the highly weathered stratum, the axial force changes little, and in the competent soil for the embedded stratum (slightly weathered stratum), the axial force of side piles decreases rapidly due to the increase of lateral friction resistance of side piles. Moreover, the axial forces of side piles increase gradually with the excavation of soil, and the change is the most drastic in the excavation about the first soil layer. This is mainly due to the loose release of soil around the side piles by the construction disturbance with the excavation of soil, and the lateral friction resistance of pile body gradually disappears, resulting in the gradual increase about the axial forces of side piles.

In Fig. 11, the bending moment of side piles under different pile spacings after the final construction of station is presented as a "bow" distribution feature with large at the middle and small at both ends, and the maximum bending moment appears near the middle part of side piles. The pile body above the excavation face of the soil is mainly strained on the excavation side of the station, but it is just the opposite in the embedded stratum at the bottom. Due to the embedded action of the bedrock at the bottom of the side piles, there is a reverse bending phenomenon, which is mainly strained on the side facing the soil behind side piles.

The axial force distribution about side piles under different pile spacings shows a "zigzags" distribution feature with large at the top and small at the bottom. The axial force changes at the excavation surface of soil and stratum interface. This is because the inside of the side piles above excavation surface about soil at the station is at the free surface of soil, and the soil around the side piles is loose and empty due to construction disturbance. The pile lateral friction provided by soil basically loses, and the axial force of side piles changes little from the top end to the bottom end. Subsequently, the axial force of side piles decreases rapidly in the pile end of embedded stratum due to the rock-socketed support and pile lateral friction.

To reveal the change rule of internal forces more intuitively about side piles with pile spacings, the largest internal forces about side piles with different pile spacings after the station construction are extracted respectively, as displayed in Fig. 12.

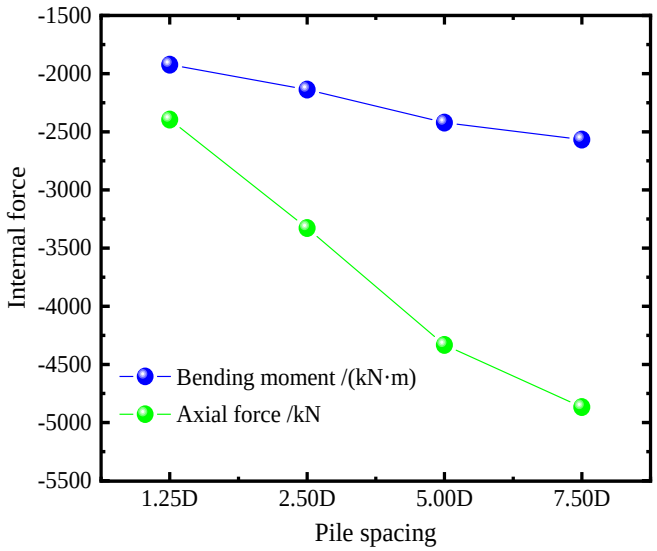

Fig. 12 Variation curve about the largest internal forces of side piles with different pile spacings

In Fig. 12, the maximum bending moment value of side piles increases with pile spacings. When pile spacing is 1.25D, 2.5D, 5D and 7.5D, the largest bending moment of side piles is -1923.49kN·m, -2137.70kN·m, -2421.67kN·m and -2566.80kN·m respectively, and the circumferential comparison increases by 214.21kN·m, 283.97kN·m and 145.13kN·m respectively. The variation law of the largest axial forces about side piles is basically like the bending moment value. The axial forces about side piles increase with pile spacings, which is also the main reason that the vertical settlement of side piles increases with the pile spacings. As the force about single pile increases gradually, the vertical settlements about side piles also increase. In addition, for pile spacing at 1.25D, the maximum bending moments as well as axial forces about side piles are -1923.49kN·m and -2395.85kN, respectively. For pile spacing at 7.5D, the largest bending moment and axial force of side pile structure are -2566.80kN·m and -4866.90kN, respectively. The bending moment as well as axial force values about side piles increase by 33.44% and 103.14% respectively, when compared with the pile spacing 1.25D. Therefore, pile spacing greatly influences the internal force about side piles and has a more obvious effect on the axial force about side piles than the bending moment.

4.3 Validation of the calculation model

The numerical calculation model can be verified for rationality through on-site monitoring or indoor model tests. Therefore, this paper conducted model tests based on the similarity ratio conversion relationship for the calculation model mentioned in this paper, and strictly excavated the soil and installed the station structure according to the numerical simulation construction sequence. Because the calculation model is symmetric, only the right half of the calculation model is selected for model testing, as displayed in Fig. 13. Apply F_x, F_y and q_{soil} through jack A, jack B, and jack C, respectively. Due to page limitations, detailed experimental design and process can refer to the previous paper (Zhang 2023). In this section, the final bending moment data of the pile body in the model test with a pile spacing of 2.50D is extracted and compared with the numerical simulation results of the corresponding calculation condition in this paper after calculating through similarity criteria, as displayed in Fig. 14.

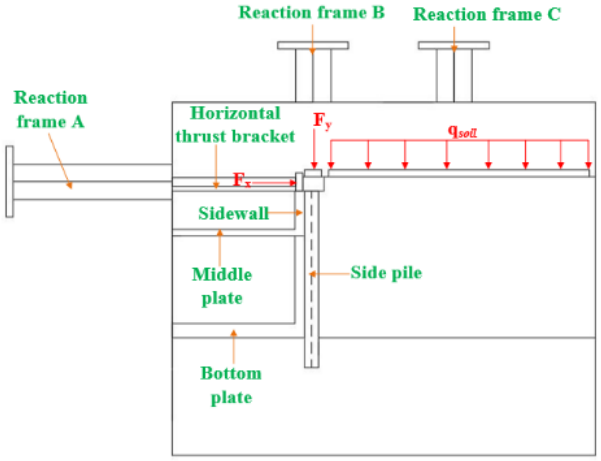

(a) Schematic diagram of the test device (after completion of the test)

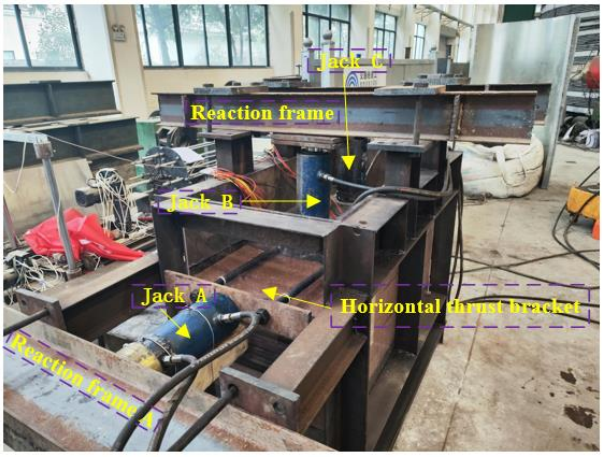

(b) Physical diagram of the test device

Fig. 13 Loading device of the model test

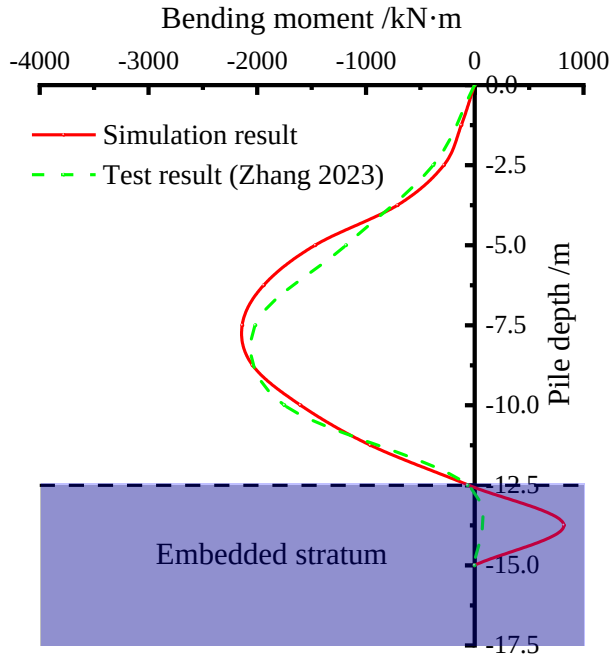

Fig. 14 Comparison curve between the results of model test and numerical simulation

From Fig. 14, it can be observed that the bending moments of the pile body in both the model test and numerical simulation exhibit a "bow-shaped (i.e., large in the middle and small at both ends)" distribution. Compared to the numerical simulation results, the bending moment results of the pile body in the model test are basically similar, but there is a slight downward trend, that is, the bending moment of the pile body embedded in the lower rock layer in the simulation is slightly greater than the test results. Although the embedded stratum of model test at the pile end are strictly configured according to similar criteria, the embedded capacity is still not as good as the slightly weathered bedrock in simulation, resulting in a slight downward development of the bending moment of the side piles. Overall, the model test results, and numerical simulation results show a good agreement, which verifies the reliability of the numerical simulation results in this paper.

5. Conclusion

(1) The formation, development, and destruction of SAE between side piles are closely related to the construction process, and the horizontal SAE between side piles is mainly formed near the excavation face where the relative displacements about soil are large. The "arch" stress concentration area appears behind the side piles, and the soil stress deflects. This part of the soil transfers the soil stress behind the arch to side piles through the arch foot, forming an effective SAE.

(2) When pile spacings are very small, the SAE between side piles exists, but it is difficult to give full play to it. When pile spacings are large, the soil arch between side piles exceeds the bearing limit and is destroyed. The SAE is very weak, and piles play a role of "longitudinal span reduction" on the free surface of soil excavation. For pile spacings between them, the SAE between side piles plays a significant role, and the side piles as well as SAE between side piles together play an effective retaining role on the soil behind the side piles in the form of a composite supporting system.

(3) The axial force distribution of side piles under different pile spacings shows a "fold line" distribution, which is large at the top and small at the bottom. The axial force changes at the excavation surface of soil and the interface of stratum. The vertical settlements about pile top increase rapidly with pile spacings. The impact of pile spacings on vertical settlement of side piles is much greater than that of horizontal displacement, and the influence on axial force of side piles is more significant than that of the bending moment.

Acknowledgments

This work was supported by the Research Project on the Key Technology of Station with the PBA Method (GL-2022-B-438) and the research and development project of the Ministry of Housing and Urban-Rural Development of the People's Republic of China (2022-K-044).

Conflicts of interest

The authors declare that there are no conflicts of interest regarding the publication of this paper.

Data Availability

The data that appeared in this paper will be available upon reasonable request.

References

Chen, C.F., Mi, W., Zhao, X.L. 2016. Bearing characteristic of composite foundation reinforced by rigid pile with cap in layered ground considering soil arching effect of high embankment. China Journal of Highway and Transport, 29(7): 1-9. (in Chinese) https://doi.org/10.19721/j.cnki.1001-7372.2016.07.001

Cheng, X.S., Liu, G.N., Gong, L.J., Zhou, X.H., Shi, B.Z. 2020. Mechanical characteristics plus differential settlement of CFG pile and cement-soil compacted pile about composite foundation under train load. Geomechanics and Engineering, 20(2): 155-164. https://doi.org/10.12989/gae.2020.20.2.155

Chen, Y.M., Xu, D.P. 2013. FLAC/FLAC3D foundation and engineering application. China Water and Power Press, Beijing. (in Chinese).

Guo, X.P., Jiang, A.N., Wang, S.Y. 2021. Study on the applicability of an improved pile-beam-arch method of metro station construction in the upper-soft and lower-hard stratum. Advances in Civil Engineering, 2021: 6615016. https://doi.org/10.1155/2021/6615016

Huang, B., Du, Y.H., Zeng, Y., Cao, B., Zou, Y., Yu, Q. 2022. Study on stress field distribution during the construction of a group of tunnels using the pile-beam-arch method. Buildings, 12(3): 300. https://doi.org/10.3390/buildings12030300

Hu, S.M. 2016. Deformation distribution control of ground settlement for cavern-pile station in Beijing metro. Journal of Beijing Jiaotong University, 40(3): 61-66. (in Chinese) https://doi.org/10.11860/j.issn.1673-0291.2016.03.011

Han, J.Y., Zhao, W., Guan, Y.P., Zhang, C.W. 2015. Deformation laws of subway station excavation by PBA method. Chinese Journal of Applied Mechanics, 32(4): 623-629. (in Chinese) https://doi.org/10.11776/cjam.32.04.B172

Kahyaoğlu, M.R., Onal, O., Imançlı, G., Ozden, G., Kayalar, A.Ş. 2012. Soil arching and load transfer mechanism for slope stabilized with piles. Journal of Civil Engineering and Management, 18(5): 701-708. https://doi.org/10.3846/13923730.2012.723353

Liu, Y.S., Huang, Y.Y. 2023. The surface settlement law of precipitation in pile-beam-arch station adjacent to pile foundation. KSCE Journal of Civil Engineering, 27: 1441-1457. https://doi.org/10.1007/s12205-023-2192-4

Liu, Q.W., Wang, M.S., Hu, S.M. 2013. Control measures for surrounding rock displacement induced by metro station construction with PBA method. China Railway science, 34(6): 61-65. (in Chinese) https://doi.org/10.3969/j.issn.1001-4632.2013.06.10

Li, T., Li, Y., Yang, T.Y., Hou, R., Gao, Y., Liu, B., Qiao, G.G. 2023. Influence of the large-span pile-beam-arch construction method on the surface deformation of a metro station in the silty clay-pebble composite stratum. Materials, 16(7): 2934. https://doi.org/10.3390/ma16072934

Lv, J.B., Lu, J.J., Wu, H. 2023. Study on the mechanical characteristics and ground surface settlement influence of the rise-span ratio of the pile-beam-arch method. Applied Sciences, 13(9): 5678. https://doi.org/10.3390/app13095678

Luo, Q.F. 2021. Study construction mechanics transformation of main structure of pile-beam-arch method of subway station. Master's thesis, Shanghai Institute of Technology. (in Chinese)

Liu, X.R., Liu, Y.Q., Yang, Z.P., He, C.M. 2017. Numerical analysis on the mechanical performance of supporting structures and ground settlement characteristics in construction process of subway station built by pile-beam-arch method. KSCE Journal of Civil Engineering, 21: 1690-1705. https://doi.org/10.1007/s12205-016-0004-9

Lai, H.J., Zheng, J.J., Zhang, R.J., Cui, M.J. 2018. Classification and characteristics of soil arching structures in pile-supported embankments. Computers and Geotechnics, 98: 153-171. https://doi.org/10.1016/j.compgeo.2018.02.007

Liu, J.F., Yu, L. 2022. Soil arch effect analysis of cohesive soil embankment on composite foundation. Journal of Ground Improvement, 4(2): 99-108. (in Chinese) https://doi.org/10.3785/j.issn.2096-7195.2022.02.002

Li, D.F., Zhao, X.Y., Hu, X.W., Ma, G.T., Liang, Y., Ma, H.S., Gao, X. 2018. Load calculation for soil nailing wall between piles basing on soil arching effect. China Journal of Highway and Transport, 31(5): 1-8. (in Chinese) https://doi.org/10.19721/j.cnki.10017372.2018.05.001

Lai, H.J., Zheng, J.J., Zhang, J. 2014. DEM analysis of "soil"-arching within geogrid-reinforced and unreinforced pile-supported

embankments. Computers and Geotechnics, 61: 13-23. https://doi.org/10.1016/j.compgeo.2014.04.007

Luo, W.L., Liu, C.W., Han, X. 2007. Numerical simulation of behaviour of piled foundation influenced by tunneling. Rock and Soil Mechanics, 28(S1): 403-407. (in Chinese) https://doi.org/10.16285/j.rsm.2007.s1.131

Liu, C.W., Han, X. 2010. Method and parameters of numerical simulation on single pile. Chinese Journal of Geotechnical Engineering, 32(S2): 204-207. (in Chinese)

Rui, R., Ye, Y.Q., Han, J., Zhai, Y.X., Wan, Y., Chen, C., Zhang, L. 2022. Two-dimensional soil arching evolution in geosynthetic-reinforced pile-supported embankments over voids. Geotextiles and Geomembranes, 50(1): 82-98. https://doi.org/10.1016/j.geotexmem.2021.09.003

Sun, J., Pei, X.K., Yang, C., Zhu, B.Z. 2023. Dynamic response analysis of the process of the utility shield tunnel under-passing the operating subway tunnel. Electronic Journal of Structural Engineering, 23(3): 44-52. https://doi.org/10.56748/ejse.234433

Wang, T., Deng, T.T., Deng, Y., Yu, X.B., Zou, P., Deng, Z.H. 2023. Numerical simulation of deep excavation considering strain-dependent behavior of soil: a case study of Tangluo Street Station of Nanjing Metro. International Journal of Civil Engineering, 21: 541-550. https://doi.org/10.1007/s40999-022-00755-8

Wang, Z. 2017. Study on horizontal pile-soil behavior of support piles in deep foundation pit in loess area based on soil arching effect. Master's thesis, Chang'an University. (in Chinese)

Yu, L., Zhang, D.L., Fang, Q., Cao, L.Q., Xu, T., Li, Q.Q. 2019. Surface settlement of subway station construction using pile-beam-arch approach. Tunnelling and Underground Space Technology, 90: 340-356. https://doi.org/10.1016/j.tust.2019.05.016

Zhao, J.P., Tan, Z.S., Yu, R.S., Li, Z.L., Zhang, X.R., Zhu, P.C. 2022. Deformation responses of the foundation pit construction of the urban metro station: a case study in Xiamen. Tunnelling and Underground Space Technology, 128: 104662. https://doi.org/10.1016/j.tust.2022.104662

Zhang, J.D. 2018. Study on stratum deformation and mechanical effect in construction of subway station by PBA. Master' s thesis, Lanzhou Jiaotong University. (in Chinese)

Zhuang, Y., Wang, K.Y. 2018. Finite element analysis on the dynamic behavior of soil arching effect in piled embankment. Transportation Geotechnics, 14: 8-21. https://doi.org/10.1016/j.trgeo.2017.09.001

Zhu, X.J., Zhao, X.L., Gong, W.M., Xu, G.P. 2014. Macro and micro-mechanism analysis of soil arching effect in the cushion of rigid pile composite foundation. Building Structure, 44(1): 82-87. (in Chinese) https://doi.org/10.19701/j.jzjg.2014.01.017

Zhao, X.Y., Wu, B., Li, D.F., Jiang, C.S., Li, Y.L., Xiao, S.G. 2016. Load calculation method for retaining wall between piles considering horizontal soil arching effects. Chinese Journal of Geotechnical Engineering, 38(5): 811-817. (in Chinese) https://doi.org/10.11779/CJGE201605006

Zhang, D.S., Zhang, X.L., Tang, H.T., Zhao, Z.Q., Guo J., Zhao, H.H. 2023. Effects of soil arching on behavior of composite pile supporting foundation pit. Computational Particle Mechanics, 10: 645-662. https://doi.org/10.1007/s40571-022-00518-1

Zhang, S. 2023. Study on the selection and construction mechanical behavior of side pile in metro station using pile-beam-arch method. Master's thesis, Southwest Jiaotong University. (in Chinese)